Study of Numerical Schemes for the CFD Simulation of Human Airways

Bholu Kumar[1*], Vivek Kumar Srivastav[2], Anuj Jain[3], Akshoy Ranjan Paul[3]

[1]Department of Mechanical Engineering, National Institute of Technology Patna, Patna, 800005, INDIA

[2]Department of Mathematics, Motihari College of Engineering, Motihari, 845401, INDIA

[3]Department of Applied Mechanics,
Motilal Nehru National Institute of Technology Allahabad, Prayagraj, 211004, INDIA

*Corresponding author

Abstract: Computational fluid dynamics (CFD) is increasingly used nowadays to capture air and particle transport in the human respiratory tract. In the present study, computer tomography (CT) scan based respiratory tract model is used for the CFD simulation. The main objective of the present study is to compare different pressure-velocity schemes (SIMPLE, SIMPLEC, PISO and COUPLED schemes) in terms of convergence and computational time. Numerical simulation is done for the three inhalation flow rates, namely 20, 40 and 60 L/min for predictions of flow phenomena inside the sixth-generation human respiratory model and also to predict the effects of flow parameters; pressures and velocity on the sixth-generation human respiratory tract. The SST k-ω model with low Reynolds number corrections is used to capture the turbulence effect. The findings will be useful for medical practitioner to understand complex airflow patterns in the human airways. Also, pressure and velocity distribution inside the human respiratory tract model will help to define the medical phenomena in core engineering terms.

Keywords: Computational Fluid Dynamics (CFD), k-ω SST turbulence model, sixth generation human respiratory tract.

1. Introduction

Nowadays, computational fluid dynamics (CFD) tools are widely used in many biological systems; human respiratory system is one of them. As, it is very difficult to know the internal flow physics of air/particle in vivo system, therefore CFD is playing vital role for an insight view of human respiratory tract using CT scan data. The realistic human airway is irregular and asymmetrical, and hence realistic results can be captured using CT/MRI data. Therefore, in present scenario researchers are concentrated on anatomical based model (CT/MRI) that reflects realistic condition of person [1]. The geometrical change has prominent effects on the CFD simulation; therefore, human airway model from CT/MRI must be studied.

Luo and Liu [2] used fifth generation CT scan model for steady state CFD simulation. It is found that laryngeal jet produced more disturbances in term of turbulence which is captured using low Reynolds number k-ω turbulence model. It was obtained that deposition of particles in CT scanned model is different from symmetrical model. Inthavong et al. reported deposition of the drugs form of micron-particle in realistic human respiratory model [3]. The study was in two-part (i) drugs delivery for normal breathing cycle (ii) drug delivery during the inhalation with breath holds (2 seconds).

Their results in terms of velocity contours and secondary flow vectors showed that vortex formation in downstream of the bifurcation indicate particle deposition. They found that breath hold allows and maximizes the local targeted deposition in first few generations. The total deposition fraction in sixth generation during inhalation phase (5 μm→ 12.9%, 10 μm→21.6%) was compared with single inhalation and breath hold (5 μm→30.1%, 10 μm→50.9%). Tian et al. performed CFD modelling of human airway to improve the delivery of inhaled pharmaceutical drugs [4]. CFD analysis has been performed for steady state inhalation condition. The airway model was extended from mouth to the fifteenth-generation bronchus. It was predicted that deposition of drugs to the targeted region can be controlled by inlet temperature and aerosol size. Elcner et al. [5] used seventh generation model for the study of influence of boundary conditions on internal flow physics. In the two-phase flow simulation of air and particle Gorji et al. [6] investigated that the maximum velocity change occurs at the larynx region of the human airways. The irregularities and bending sections of the realistic model causes higher turbulence and these regions are highly prone to particle trap at higher flow rates. Lintermann and Schroder [7] performed two cases of flow simulation. In the first investigation, large and heavy particles with a diameter of 100 microns and in the second investigation small particle mixture with diameter 2.5-10 microns were simulated. It was investigated that the most of the heavier particles deposited in the upper respiratory tract and at the bifurcations itself. However, lighter particles penetrate the human lung below the sixth generation and may cause the lung injury.

Selection of appropriated turbulence model is an essential aspect for accurate capturing of the flow physics due to turbulence. The two-equation k-ε Realizable turbulence model is frequently used in high-speed flow in the recent past [8-9]. The standard k-ε model is not recommended due to its larger dispersion. Zhang and Kleinstreuer [10] suggested the LRN k-ω model, but Jayaraju et al. [11] later suggested the SST k-ω model. Mihaescu et al. [12] compared k-ε, k-ω and LES models in a realistic pharyngeal airway model and found differences of 45% between the k-ε and the LES mean axial velocities calculated in the pharynx region [10-12]. These differences were much lower (within 30%) in the case of the k-ω model. Most of the published CFD results were obtained for steady inspiration which is understandable because of the enormous computational time needed to simulate an entire breathing cycle [13].

It is found from the literature survey that limited researchers have used CT scan model in the recent past and most of the studies were concentrated either on two-phase study or boundary conditions. However, comparisons of different numerical schemes have not been reported till now. Therefore, present study is concentrated on comparison of different pressure-velocity schemes in terms of computational time. The comparison of different models will help to select the optimum pressure-velocity schemes in case of human respiratory model.

2. Methodology

Three dimensional reconstruction of sixth generation human airways is done from CT-scan images. The computational geometry is constructed from CT-scan of a healthy non-smoking male.
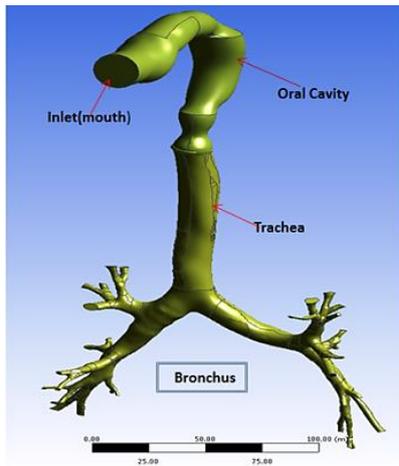

**Fig. 1 - CT scan based Human Respiratory Tract**
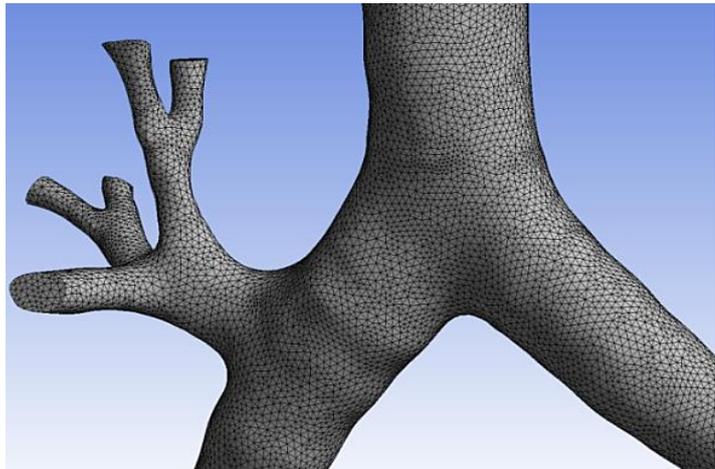
Fig. 2 - Computational grid of Human Airways

The computational model is extending from oral cavity (mouth of human respiratory tract) to the sixth generation of human respiratory model. Initially, the CT scan images (DICOM file) are imported into the MIMICS software which is the strong image processing software where all slices are segmented and exported in STL (Standard Tessellation Language) format. The STL format of the model from the MIMICS is imported into the Solid-works software for further modification in the computational geometry. Thereafter, the computational model is imported into the ANSYS design

modular (Fig.1). The equivalent diameter of outlet cross-sections of sixth generation human airways lies from 1.17 mm to 5.45 mm.

2.1 Grid Generation

The meshing of the computational model is generated into the ICEM module of the ANSYS workbench with tetrahedral elements, which is most suitable and appropriate for this model. The maximum skewness is found to be 0.86 which is obtained by huge effort and refinement. The grid independency test is achieved at the grid size of 3,538,213. The maximum velocity and area-average velocity are evaluated on XZ plane at the vertical location of Y = 0.098 m for the grid independence test. The grid generation and grid independency test (GIT) of the computational model is given in the Fig. 2 and Tables 1and 2 respectively.

Table 1 - GIT with reference to maximum velocity

Case	Number of Elements (in Millions)	Maximum velocity, V_{max} (m/s)	Percentage change in V_{max}
I	1.9	12.00	-
II	2.8	12.10	0.87
III	3.5	12.00	0.82
IV	5.1	11.93	0.58

Table 2 - GIT with reference to area-average velocity

Case	Number of Elements (in Millions)	Area average velocity, V_{avg} (m/s)	Percentage change in V_{avg}
I	1.9	9.88	-
II	2.8	10.03	1.50
III	3.5	9.67	-3.67
IV	5.1	9.75	0.79

2.2 Governing Equations

The air flow is assumed to be steady and incompressible.

2.2.1 Continuity Equation

Since flow has been assumed to be steady and incompressible therefore,

$$\frac{\partial u_j}{\partial x_j} = 0 \tag{1}$$

2.2.2 Momentum Equation

$$\frac{\partial \left(u_i u_j \right)}{\partial x_j} = -\frac{1}{\rho}\frac{\partial p}{\partial x_i} + \frac{\mu}{\rho}\frac{\partial^2 u_i}{\partial x_j \partial x_j} \tag{2}$$

Where, μ = coefficient of dynamic viscosity u_i, u_j (i, j= 1, 2, 3) is the velocity component in x, y and z-direction. p = pressure, ρ = density of fluid.

2.2.3 Turbulence Model

The transport equations for k (turbulent kinetic energy) and ω (specific turbulent dissipation rate) is k-ω turbulent model are:

$$\overline{u}_j \frac{\partial k}{\partial x_j} = \tau_{ij}\frac{\partial \overline{u}_i}{\partial x_j} - \beta^* k\omega + \frac{\partial}{\partial x_j}\left[(v + \sigma_k v_T)\frac{\partial k}{\partial x_j} \right] \tag{3}$$

$$\overline{u}_j \frac{\partial \omega}{\partial x_j} = \alpha\frac{\omega}{k}\tau_{ij}\frac{\partial \overline{u}_i}{\partial x_j} - \beta\omega^2 + \frac{\partial}{\partial x_j}\left[(v + \sigma_\omega v_T)\frac{\partial \omega}{\partial x_j} \right] \tag{4}$$

Where, v, v_T and τ_{ij} are kinetic molecular viscosity, turbulent viscosity, and Reynolds stress tensor respectively.

Here, $v_T = C_\mu f_\mu k / \omega$ and the function, $f_\mu = \exp\left[-3.4 / (I + R_T / 50)^2 \right]$ with R_T= k/μω, μ is dynamic molecular viscosity. The Model constants are:

$$C_{\mu} = 0.09, \alpha = 0.555, \beta = 0.8333, \beta^{*} = 1 \ and \ \sigma_{k} = \sigma_{w} = 0.5$$

2.3 Boundary Conditions

The velocity inlet and pressure outlet boundary conditions are respectively applied at the inlet and all 32 outlets of the human airways. Laminar and turbulence models are applied depending upon the type of air flow, based on the numerical value of Reynolds number. The SST k-ω turbulence model is applied for the turbulent flow. The enhanced wall function with no slip is applied at the walls of the human airways. The numerical investigation is carried out for the flow rates of 20, 40, and 60 L/min respectively. The properties of air at normal conditions are taken in this study, i.e. density of 1.225 kg/m^3 and dynamic viscosity of 1.78×10^{-5} N-s/m^2.

2.4 Numerical Simulation

Numerical simulation is carried out by the FLUENT solver of the ANSYS software. The simulations are carried out for the pressure-velocity coupling schemes, namely SIMPLE, SIMPLEC, PISO, and COUPLED. The simulation was converges after 11000 iterations with the convergence criteria of 1×10^{-4}. The pressure and momentum term was discretized by 2nd order upwind scheme. The computational work is run on the IBM blade server, having eight blades with 32 GB RAM and Octa-core processors for each blade.

2.5 Computational Validation

In the present study, CFD validation is carried out with the computational results presented by Nowak et al. [14]. For their study, they have used simplified model given by Weibel [15]. For the same respiratory model and boundary conditions, velocity profile is evaluated at the mid plane of 4th generation. The validation is shown in Fig. 3, which is within the acceptable limit. This validation is performed for the inspiratory flow rate of 40 L/min.
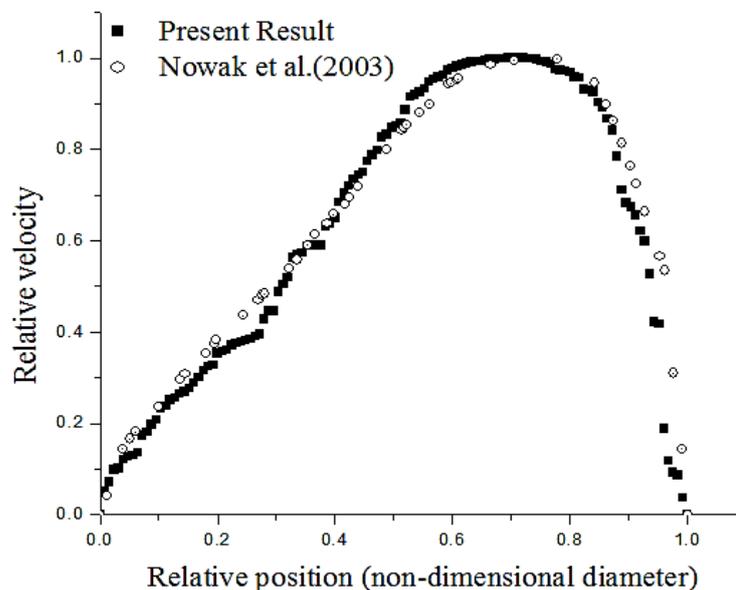

Fig. 3 - Relative velocity at mid-section of bronchus-4.

3. Results and Discussion

3.1 Measurements of type of flow (Reynolds number at the different locations of the Human Airways):

It is well known that in the case of pipe flow, flow less the Reynolds number (Re) of 2000 is termed is laminar flow and the flow with Re > 4000 is termed as turbulent flow. However due to the irregularities and cartilages rings presence in the human respiratory tract the flow becomes turbulent with the smaller value of Reynolds number as compared to the typical circular ducts. Reynolds number corresponding to different flow rates are analyzed and reported in table 3. Reynolds number is computed at different locations of the airway model which is shown in the Fig. 4. It is found that at 20 L/min of inspiratory flow rate, the flow is laminar throughout the airway model. However, for 40 and 60 L/min, flow is turbulent in most of the locations. It is anticipated that even the flow is laminar but due irregularity in the human respiratory tract the flow becomes turbulent. It is observed that in spite of being laminar flow at 20 L/min of inspiratory flow rate, it took same computational time as compared to turbulent flow in 40 & 60 L/min of inspiratory flow rate.
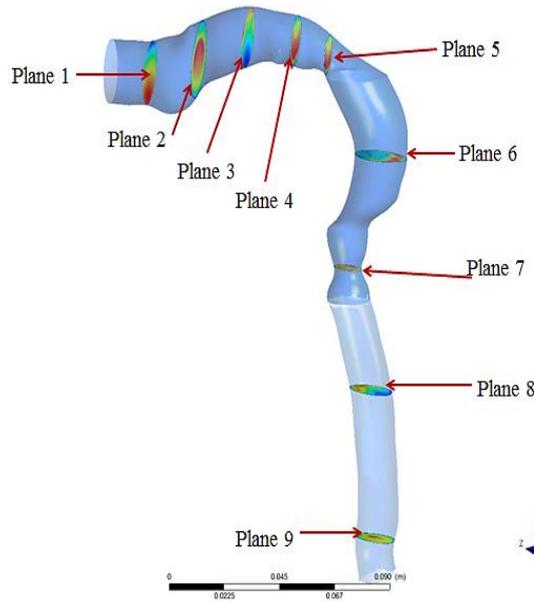
Fig. 4 - Different planes for analyzing the flow variations in the human respiratory tract

3.2 Comparison of Pressure-Velocity Coupling Schemes:

The computational simulation at the inspiratory flow rate of 60 L/min is carried out one-by-one using the pressure velocity coupling scheme of SIMPLE, SIMPLEC, PISO, and COUPLED. The simulations are run for the total number of ten thousand iterations with the convergence criteria of $1x10^{-4}$. It is observed that the computational simulations achieve their convergence in order of $6x10^4$ to $10x10^4$ iterations respective to the applied pressure-velocity coupling schemes. Among all the four schemes it is investigated that the similar results are executed from all the schemes. However, the PISO scheme takes the least computational time in comparison with other schemes for the same results and therefore, PISO scheme is adopted for further investigations. The comparison of these four computational schemes is shown in the Table 4, Table 5, Fig. 5, and Fig. 6.

Table 3 - Type of flow at the different cross-sections of the human respiratory tract

Cross-section	Reynolds Number at 20 L/min	Reynolds Number at 40 L/min	Reynolds Number at 60 L/min
Inlet	1328	2656	3985
Plane 6	1896	3542	5129
Plane 7	2617	5163	7764
Plane 8	1872	3694	5444
Plane 9	1795	3602	5385

Table 4 - Comparison among SIMPLE, SIMPLEC, PISO, and COUPLED pressure-velocity coupling schemes at YZ-plane with X = 0.077 m

Pressure-Velocity Coupling Scheme	Area average Velocity (m/s)	Maximum velocity (m/s)	Computing Time (hours)
SIMPLE	4.12	11.08	16.56
SIMPLEC	4.02	10.82	17.31
PISO	4.15	10.66	14.60
COUPLED	4.15	10.82	22.98

The maximum local velocities are computed at five different locations of human airways for these four pressure-velocity coupling schemes. It is depicting from Fig. 5 & Fig. 6 that the maximum local and average velocity is almost same for all the schemes. It is found that computational time for PISO scheme is 14.6 hours. However, for the similar conditions, SIMPLE, SIMPLEC and COUPLED schemes took 16.56, 17.31 and 22.98 hours respectively. Thus due to least computational cost for the similar results, PISO scheme is selected for the further investigations.

Table 5 - Comparison among SIMPLE, SIMPLEC, PISO, and COUPLED pressure-velocity coupling schemes at XZ-plane with Y = 0.10 m

Pressure-Velocity Coupling Scheme	Area average Velocity (m/s)	Maximum velocity (m/s)	Computing Time (hours)
SIMPLE	10.04	11.66	16.56
SIMPLEC	9.99	12.31	17.31
PISO	10.00	11.76	14.60
COUPLED	10.05	11.89	22.98
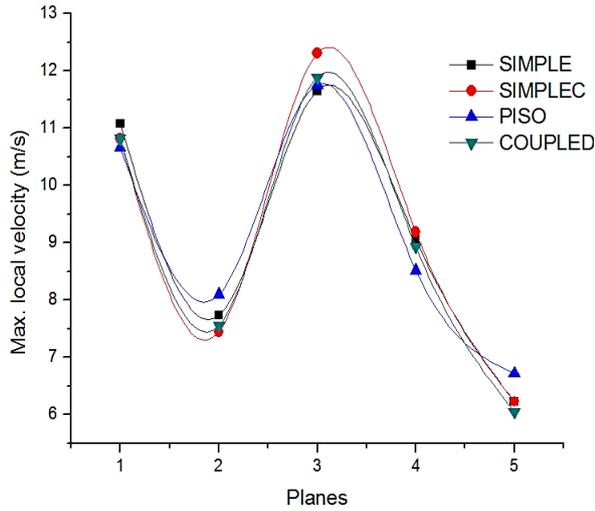
Fig. 5 - Plot of maximum local velocity at different locations corresponding to different Pressure-velocity schemes
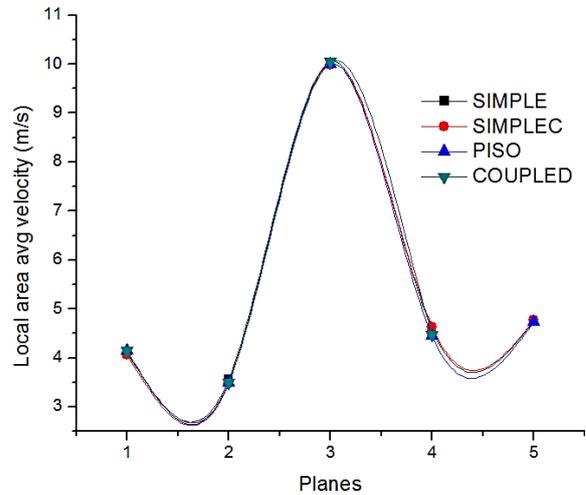
Fig. 6 - Plot area average velocity on Planes YZ and XZ for different pressure-velocity coupling schemes.

In above figures (Fig. 5 and Fig. 6) the points on the X-axis (1-5) are indicating the Planes YZ at X = 0.077 m, Plane XZ at Y = 0.14 m, 0.10 m, 0.06 m and 0.01 m respectively.
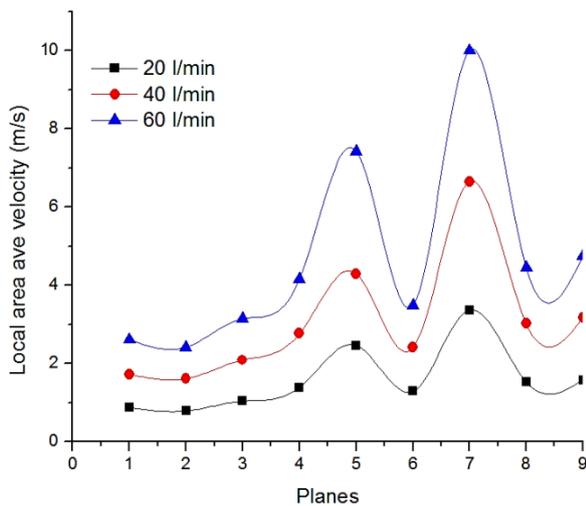
Fig. 7 - Plot of area average velocity at the different locations of the Human airways, from planes 1 to 9.
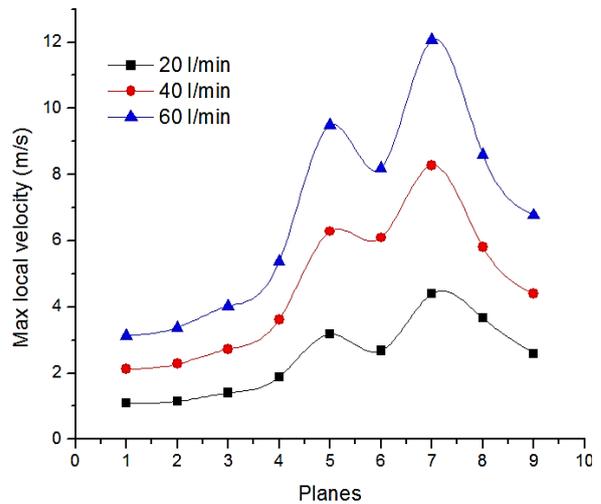

Fig. 8 - Plot of local maximum velocity at the different locations of the Human airways, from planes 1 to 9.
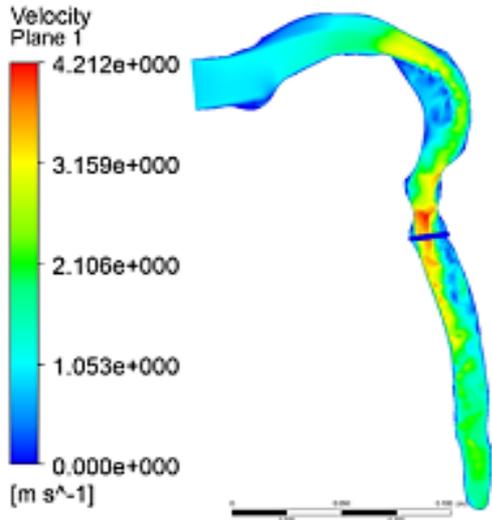
Fig. 9 - Velocity contour at flow rate of 20 L/min
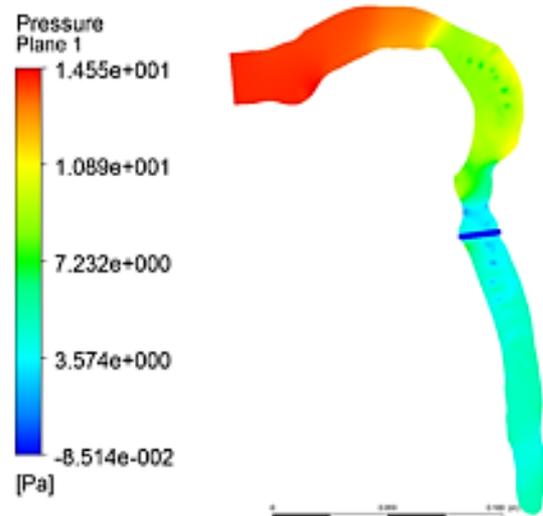

Fig. 12 - Pressure contour at flow rate of 20 L/min
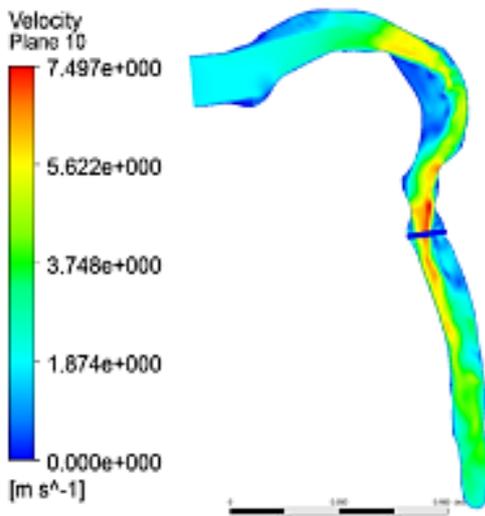
**Fig. 10 - Velocity contour at flow rate of 40 L/min**
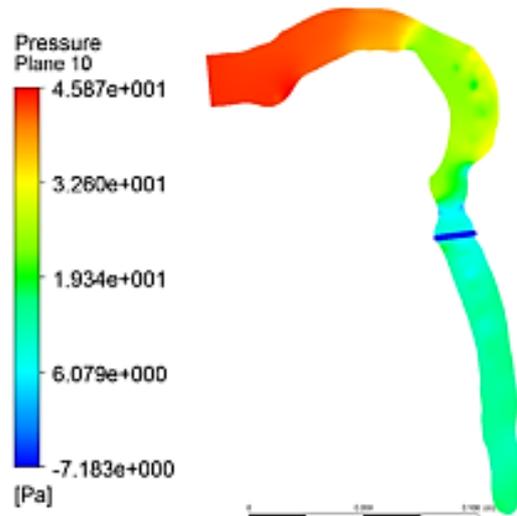

Fig. 13 - Pressure contour at flow rate of 40 L/min
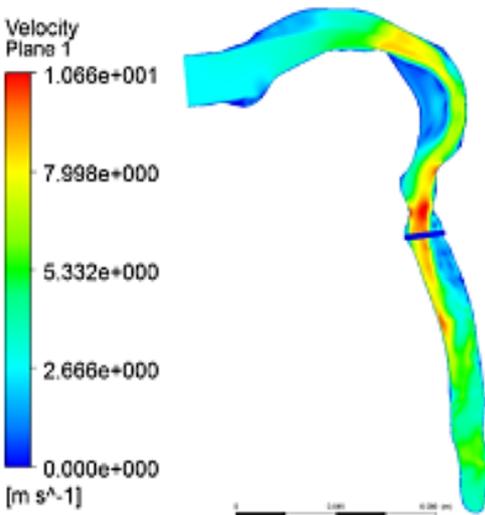
**Fig. 11 - Velocity contour at flow rate of 60 L/min**
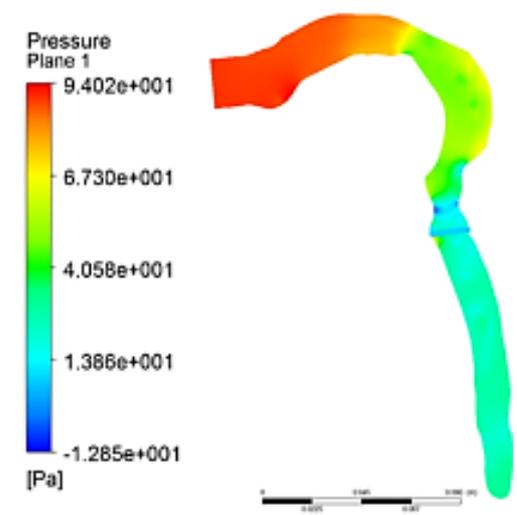
Fig. 14 - Pressure contour at flow rate of 60 L/min

3.3 Velocity distribution from inlet of mouth to the sixth generation of human airways:

The velocity variation is evaluated for the three flow rates (20, 40, and 60 L/min) at different locations of human airways which is depicted from the Fig. 4. The local area average velocity is computed at different planes which is shown in the Fig. 7. It is seen from the graph that peak values of area average velocity are found at planes 5 and at plane 7 corresponding to 60 L/min of inhalation flow rate. In comparison to the other planes, these values are maximum at plane 5 & 7 because of minimum cross-sectional area. The max local velocity is computed at different planes and is shown in Fig. 8. The maximum local velocity is occurred at plane-7 due to reducing of cross sectional area. It is seen that the disturbances in the air flow pattern occur from plane 4 to 8. It is seen from the Fig. 8 and Fig.9 to Fig.11 that larynx region has prominent disturbance in comparison of the other locations. As the flow rates increases from 20 L/min to 60 L/min, velocity magnitude as well as area of disturbance increases near the larynx region. Thus, it is anticipated that during the running or exercise condition, high flow disturbance occurs near the larynx region due to sudden reduction in the cross-section area. This disturbance in the path leads the phenomena of turbulence. It is also expected that because of high velocity near the epiglottis region, velocity gradient may high and therefore peak-wall shear stress in this region. This peak values may create wall injury. It is well known that the flow in the human lungs occur due to the pressure difference process. During the inhalation, pressure of inlet (at the inlet of oral cavity) is higher in comparison of outlet (outlet of lower generation bronchus), so that the flow moves from inlet to outlet. The pressure contours for three inhalation flow (20, 40 and 60 L/min) rates is shown in Fig. 12 to Fig. 14. Higher pressure is observed in the upper part of the oral cavity due to minimum velocity. However, lower pressure is found in the lower part of the oral cavity and this keep on reducing as it moves towards the lower parts of the lungs.

3.4 Computational flow visualizations using velocity and pressure contours:

The velocity and pressure contours (Fig.9 to Fig. 14) are computed at the vertical mid-plane of the human airways respectively for the inspiratory flow rates of 20, 40 and 60 L/min. It is clearly evident from the velocity and pressure contours that the maximum velocity and pressure changes occur at the larynx region of the human airways. The strength of laryngeal jet increases with increasing inspiratory flow rates. During the inhalation more pressure is reported in the upper respiratory tract as compared to the lower respiratory tract and increasing level of pressure is also seen in upper respiratory tract with increasing rate of inspiratory flow rates.

4. Conclusions

In the present study, CT scan model have been used for the airflow study. The comparative analysis is carried out among the four pressure-velocity schemes namely, SIMPLE, SIMPLEC, PISO and COUPLED schemes at the inspiratory flow rate of 60 L/min in order the minimize the computational cost. Thereafter, computational simulations with appropriated pressure-velocity coupling schemes are carried out for the insight understanding of dynamics of airflow into the human respiratory tract. It is found that PISO pressure-velocity coupling scheme takes least time of convergence as compared to other schemes for the similar results. Higher velocity variation is reported in the oral cavity as compared to the other locations of the human respiratory tract. A laminar flow with flow rate of 20 L/min at inlet (i.e. at the mouth) becomes turbulent in larynx section of the oral cavity due to the irregularities and the presence of cartilage rings of the human airways. From the plot of velocity at the different locations of the Human airways and flow visualization from the contours of velocity and pressure, it is concluded that the peak velocity gradient occurs in oral cavity and bifurcation junctions that may leads to wall injury. It is also noted the PISO pressure velocity coupling scheme compete the other schemes with similar results at the flow rates of 60 L/min (heavy breathing condition), therefore PISO scheme is suitable in higher breathing condition. However, further investigations need to perform in future to check the suitability of PISO scheme in light breathing (15 L/min) and in normal breathing (30 L/min) conditions.

Acknowledgement

References

[1] C, Kleinstreuer., and Z, Zhang (2010). Airflow and Particle Transport in the Human Respiratory System. Annual Review, Fluid Mechanics, 42, 301-334.

[2] H.Y, Luo., and Y, Liu (2009). Modeling the bifurcation flow in CT-scanned human lungs airways. Journal of Biomechanics, 42, 1869-1876.

[3] Kiao, Inthavong., Lok-Tin, C., Jiyuan, T., Songlin, D., and Francis, T (2010). Micron particle deposition in a tracheobronchial airways model under different breathing conditions. Medical Engineering and Physics, 32, 1198-1212.

[4]   Geng, T., Philip Worth, L., Guoguang, Su., and Michael, H (2014). Characterization of Respiratory Drug Delivery with Enhanced Condensation Grothusing an Individual Path Model of Entire Tracheobronchial Airways. Annals of Biomedical Engineering, 39, 1139-1153.

[5]   Jakub, E., Michaela, C., and Miroslav, J (2014). The influence of boundary conditions to the flow through model of upper part of the human respiratory system. EDP web of Conferences., 67, 20-25.

[6]   Gorji, M.R., Gorji, T.B., and Gorji, B.M (2016). Details of regional particle deposition and airflow structures in a realistic model of human tracheobronchial airway: two-phase flow simulation. Computers in Biology and Medicine, 74, 1-17.

[7]   Lintermann, A., and Schroder, W (2017). Simulation of aerosol particle deposition in the upper human tracheobronchial tract. European Journal of Mechanics B/Fluids, 63, 73-89.

[8]   Azamahani S., Nurul Akma Mohd Y., Saiful Anuar Abd H., Al Emran Ismail, Salihatun S., Sufizar A., Mohd Nasrull Abdol R., Shahruddin M., and Sallehuddin Shah A (2018). A Comparative Study of Turbulence Models on Aerodynamics Characteristics of NACA0012 Airfoil. International Journal of Integrated Engineering, 10 (1), 134-137.

[9]   Lohia, Devendra K., Kumar, B., Srivastava, S., and Paliwal, H.K (2018). Numerical Simulation of Supersonic Over-expanded Jet from 2-D Convergent-Divergent Nozzle. International Journal of Integrated Engineering, 10 (8), 195-201.

[10] C, Kleinstreuer., and Z, Zhang (2003). Laminar-to-turbulent fluid-particle flows in human airway model. International Journal of Multiphase Flow, 29, 271-289.

[11] S.T, Jayaraju., M, Brouns., S, Verbanck., and C, Lacor (2007). Fluid flow and particle deposition analysis in realistic extrathoracic airway model using unstructured grids. Journal of Aerosol Science, 38, 494-508.

[12] Mihai, M., Shanmugam, M., Maninder, K., Sid, K., and Ephraim, G (2008). Large Eddy Simulation and Reynolds-Averaged Navier-Stokes modeling of flow in a realistic pharyngeal airway model: An investigation of obstructive sleep apnea.Journal of Biomechanics, 41, 2279-2288.

[13] Pejman, Farhadi G., Erfan, K., Omid, A., Abolhassan, F., Jiyuan, Tu., and Alireza, S (2012). Numerical analysis of micro-and nano-particle deposition in a realistic human upper airway.Computers in Biology and Medicine, 42, 39-49.

[14] Natalya, N., Prashant P, Kakade., and Ananth V, A (2003). Computational Fluid Dynamic Simulation of Airflow and Aerosol Deposition in Human Lungs.Annals of Biomedical Engineering, 31, 374-390.

[15] E.R, Weibel (1963). Morphometry of human lungs.Springer Verlag and Academic Press, Berlin, New York.